Dynamics of laser-produced Sn-based plasmas for a monochromatic 13.5 nm extreme ultraviolet source

Y. Tao[*1, 2], M. S. Tillack[1, 2], K. L. Sequoia[1, 2], R. A. Burdt[2,3], and F. Najmabadi[2, 3]
[1]Department of Mechanical and Aerospace Engineering,
[2]Center for Energy Research,
[3]Department of Electrical and Computer Engineering
University of California, San Diego. 9500 Gilman Drive, La Jolla, CA, USA 92093-0417

ABSTRACT

Dynamics of laser-produced Sn-based plasmas were investigated for a monochromatic EUV lithography (EUVL) source. A hollow plasma density in a Sn plasma driven by Nd:YAG laser was observed in the late time within the laser pulse. The possible reason comes from the distributed laser energy deposition in the expanding corona. This distributed absorption results in a temperature gradient in the corona and a broad EUV spectrum. It was shown that for CO_2 laser most of the laser energy deposition is localized around the critical density, a narrower EUV x-ray spectrum and a higher conversion efficiency from laser to monochromatic 13.5 nm EUV emission can be expected. It was found that 0.5% Sn-doped foam targets show an almost the same electron density as compared with that of solid density Sn targets. The same n_e enables efficient absorption of laser energy, and at the same time much lower Sn ion number density results in less re-absorption of the in-band 13.5 nm EUV emission induced by the plasma itself, so high CE can be expected with a low concentration of Sn.

Keywords: laser plasma, dynamics, EUV

1. INTRODUCTION

Pulsed laser-produced plasma has been used as compact x-ray (ranging from several 10 eV to 100 keV) light sources for a long time, especially in recent time as a promising candidate light source for extreme ultraviolet lithography (EUVL). EUVL is an emerging technology as the next generation lithography tools used in semiconductor industry to produce electronic node with feature size of 32 nm or smaller. Development of a powerful and clean EUV light source is still one of the critical challenges to apply EUVL to high volume manufacturing (HVM). Most of the efforts in the development of an EUV source focus on monochromatic (2% bandwidth) 13.5 nm matching with the only available EUV optics-multilayer Mo/Si mirror. Sn has been considered as the most promising fuel for the EUV source because of its high conversion efficiency (CE) from laser to monochromatic 13.5 nm. Laser produced Sn plasma has shown the highest CE and scalable EUV power. However, further understanding of the fundamental plasma physics is still necessary to enhance CE and mitigate debris [1].

Even though LPP has been studied for more than 40 years, because of high atomic number and steep gradient in temperature and density profiles laser-produced Sn plasma has never been understood completely, especially for the plasma physics under the particular conditions favorable for monochromatic 13.5 nm EUV emission. Due to the scarcity of accurate atomic data of Sn at high temperature, it is extremely complicated to simulate the generation and transport of EUV light in Sn plasma simply using existing numerical models. It is necessary to carry out detailed measurements to understand the plasma physics and to benchmark models.

Due to the opacity of Sn plasma, the final output of 13.5 nm EUV light is a result of a trade-off between its generation and re-absorption induced by plasma itself [2]. So an optimized plasma density profile, which is needed for efficient generation and less absorption of EUV light, is essential optimization of the parameters of the driving laser pulse and target to enhance in-band CE. At the same time, the initial density profile is a key factor to determine the final ion energy achieved from the electric field setup by plasma expansion. And the laser-plasma interactions take place in an expanding corona blowing off from an irradiated target. The plasma density and temperature profiles affect the mix of

* yetao@ucsd.edu; phone 1 858-822-1036; fax 1 858-822-2120

Ultrafast X-Ray Sources and Detectors, edited by Zenghu Chang, George A. Kyrala, Jean-Claude Kieffer,
Proc. of SPIE Vol. 6703, 67030A, (2007) · 0277-786X/07/$18 · doi: 10.1117/12.731032

the interaction processes. In turn, the interactions significantly modify the plasma profiles. So it is very important to characterize the dynamic plasma density profile and to understand and to optimize the EUV plasma.

Varying the parameters of the lasers pulse is a convenient way to optimize the profiles of density and temperature of plasma. Various lasers with different wavelength, pulse duration, focal spot size, and intensity have been employed to generate the in-band EUVL source [3-6]. Q-switched Nd:YAG laser is most widely used in the past decade due to its wide availability, good beam quality, and manageable pulse duration. However, in recent time, CO_2 laser has been considered as a main laser driver for EUVL source by industry due to its high CE, relatively low cost, and commercially available high power[7]. Another way to control plasma properties is to optimize target design. It has been shown that the reduction of Sn concentration could significantly reduce the Sn debris and Sn consumption while keeping high in-band CE[8].

In this paper, we will present the investigations on the dynamics of laser-produced Sn-based plasma. 2-D density map of laser-produced Sn plasma is deduced from the observed interferograms. Laser absorption mechanisms in Sn plasma driven by Nd:YAG and CO_2 lasers are analyzed according to the measured plasma density. The effect of laser absorption mechanism on the generation of EUV emission is discussed. Plasma density profile of low concentration Sn-doped foam target is measured and compared with solid density Sn.

2. EXPERIMENTAL ARRANGEMENT

The experimental arrangement used in present experiments has been described in a previous work[9]; only a simple introduction is given here. A commercial Nd:YAG laser (Continuum Surelite II) is employed to generate the EUV plasma , the laser has a wavelength of 1.06 μm and a standard pulse duration of 7 ns. In present experiments, a 10 ns pulse duration is obtained by shifting the delay time between the trigger signals for flash lamp and Q-switch off the optimum value. The focal spot size of the laser pulse is kept constant at 110 μm .

Pure Sn slab and low density Sn-doped foam are used in present experiments. The foam target is fabricated as the follows [10]. The required amount of tin oxide is dispersed into resorcinol formaldehyde (100mg/cc) solution and dried. The concentration of tin and its uniformity are confirmed by a scanning microscope. The concentration of tin in foam varies from 0.5 to 1 %. The foam target has a diameter of 500 μm.

The plasma density profile is measured using a Nomarski interferometer. A small part split from the pumping pulse is converted into 0.532 μm light by a second harmonic generator (SHG) (type II KDP crystal) and used as a probe beam. A l/2 wave plate and a cube polarizer are used to adjust the polarization and energy of the probe beam. The probe beam passes through the plasma parallel to the target surface and is relayed to an imager by a F/15 lens. The Nomarski interferometer is inserted in front of the imager. The interferogram is recorded by an intensified CCD (ICCD) camera (Princeton, PI-MAX), whose gate interval is always 2 ns. The gate is triggered by the DG535 with a suitable delay with respect to the lasers. The spatial resolution of the interferometer is better than 20 μm with a magnification of 7×. A multilayer interference filter is placed in front of the ICCD camera to block the strong broadband emission from the plasma.

3. RESULTS AND DISCUSSIONS

3.1 Dynamics of solid density Sn plasma

Density profiles of laser-produced plasma at various times within the driving laser pulse were observed by the temporally resolved Nomarski interferometer. Typical interferograms achieved at delay times of –3, 0, and 3 ns with respect to the peak of the laser pulse are shown in Fig. 1. Laser is incident from the right hand side in the interferograms shown in Fig.1. The laser intensity is 2×10^{11}W/cm^2. Solid density Sn slab is used in this experiment. Initial target surface is marked by a dashed white line as shown in Fig.1. Reference interferograms are recorded before the laser irradiation and used to get phase shift induced by the plasma.

The opaque region between the target surface and the fringes comes from the fact that the probe beam only can propagate in the plasma with a density below the critical density of the probe beam. Another contribution to the opaque region is the refraction of the probe beam induced by plasma density gradient along the line of the probe beam. It is obvious that the critical density surface moves into vacuum with increase of time. This is well-known longitudinal thermal plasma expansion. In addition to the longitudinal expansion lateral expansion of the plasma is also seen in Fig. 1. This lateral expansion comes from the finite focal spot size of the laser beam in the present experiment.

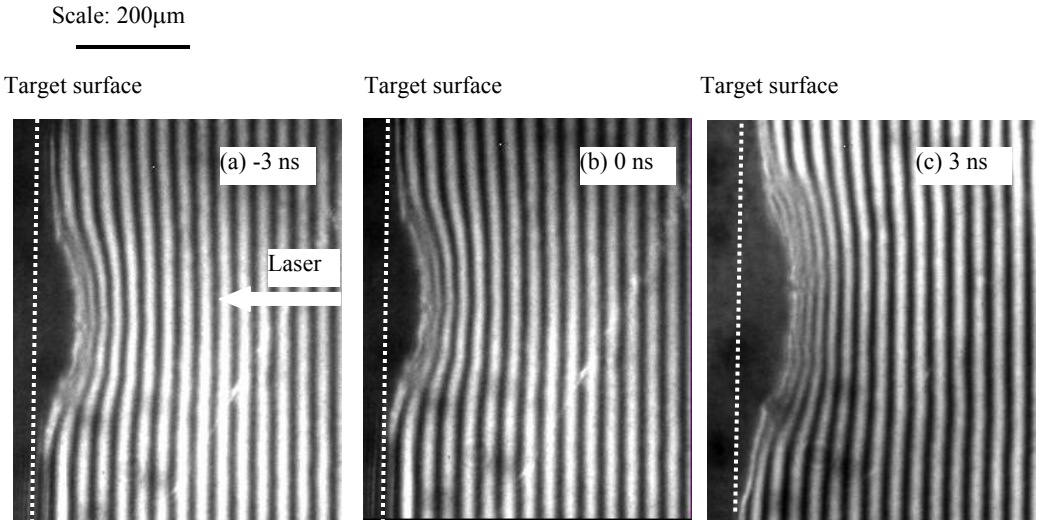

Fig.1 Interferograms of laser produced solid Sn plasmas observed at delay times of (a) –3, (b) 0, and (c) 3ns respectively with respect to the peak of the laser pulse.

Phase shift induced by the plasma was deduced from the interferograms shown in Fig.1 and the reference interferograms with a mathematical treatment based on fast Fourier transform (FFT) [11]. The phase map obtained from the interferograms shown in Fig. 1 (a), (b), and (c) are shown in Fig.2 (a), (b), and (c) respectively. The line profiles along the dashed lines are plotted under the phase map. The lateral expansion can obviously be seen in the phase shift maps shown in Fig. 2.

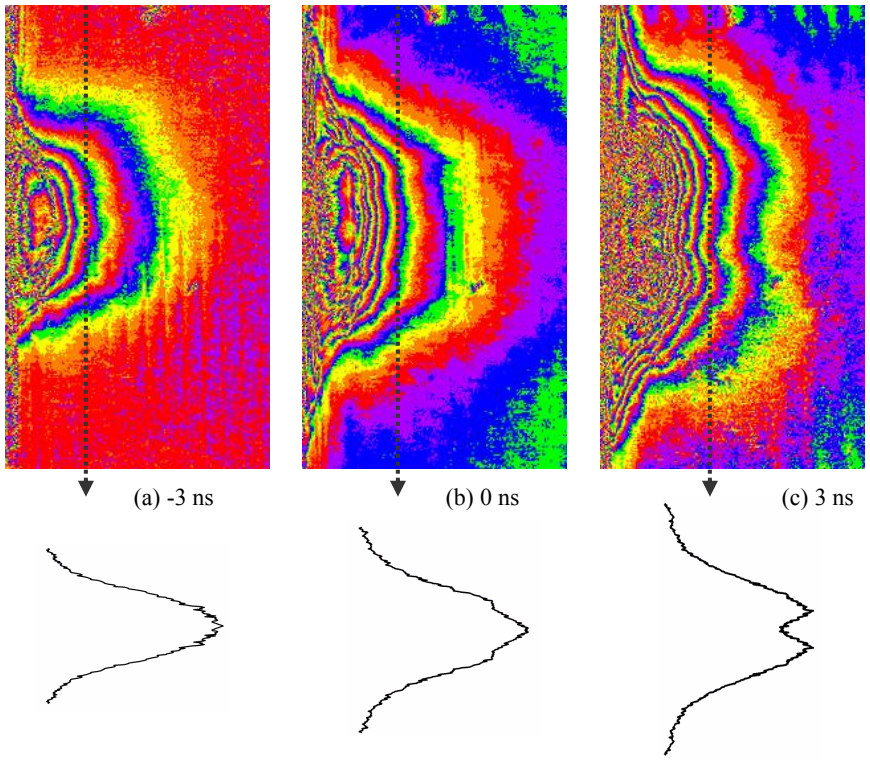

Fig.2 Phase shift map of laser produced solid Sn plasmas observed at delay times of (a) –3, (b) 0, and (c) 3ns.

It is also worth noting in Fig. 2 (c) that the phase shift profile along the dashed line is different from those shown in Fig. 2 (a) and (b). The phase profiles in Fig. 2 (a) and (b) have a Gaussian-like shape, the peak is located at the center. However, at 3 ns, a dip appears at the center. It is well known that laser-produced plasma obeys cylindrical symmetry. An illustration of the diagnostics is shown in Fig.3. The pumping laser beam is incident along x. The probe beam propagates along y. The plasma has cylindrical symmetrical with respect to x. The refractive index of plasma can be described as $n(x,r)$, where r represents the distance to x. It is seen that the central part of the probe beam experiences the maximum thickness of plasma, and the cylindrical symmetry makes the central part of the beam experiences all density regions. So the central part should have a maximum phase shift. We will discuss the possible reason for the dip in phase profile at late time of laser pulse later after the density map is obtained.

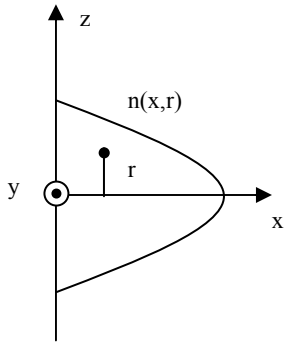

Fig.3 Geometry of diagnostics

A 2-D Plasma density map was extracted from the phase shift map shown in Fig. 2 using Abel inversion. The density contour of Sn plasma at –3, 0, and 3 ns with respect to the peak of laser pulse are shown in Fig. 4. It is seen in Fig.4 that at –3 and 0 ns the lateral plasma density has a Gaussian distribution, the highest density appears at the center. However, at 3 ns, there are two peaks off the center. The dip at the center is obvious.

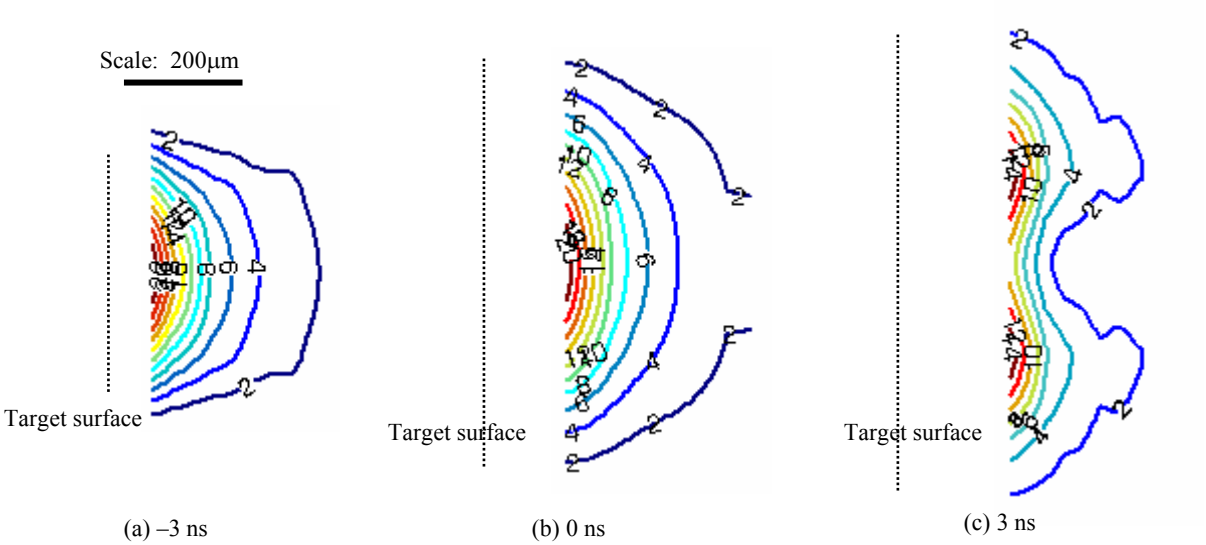

Fig 4. Contour of electron number densities of Sn plasma observed at various times of (a) –3, (b) 0, and (c) 3 ns respectively.

Plasma density profiles along the line of laser incidence are drawn in Fig.5. Black squares represent the data observed at –3 ns. Red dots and blue triangles correspond with 0 and 3 ns respectively. It is seen that data at –3 and 0 ns can be fitted with decaying exponential functions, however the data at 3 ns deviate from a decaying exponential function.

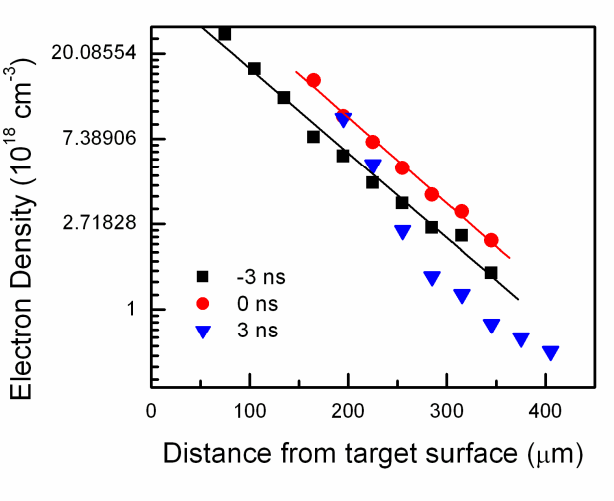

Fig.5 Plasma density profiles along the line of laser incidence observed at various delay times of (a) –3 (black square), (b) 0 (red dot), and (c) 3 ns (blue triangle) respectively.

Now we start to discuss the possible reason for the anomalous plasma density observed at late time of laser pulse. Under the laser intensity used in present experiments, plasma density steeping induced by ponderomotive can be neglected. The possible reason comes from different mechanism of laser energy deposition at different times of laser pulse. For EUVL source experiment, the optimum value for the product of laser intensity and the square of wavelength $I\lambda^2$ is around 10^{11} W/cm^2. Within this intensity range, inverse Bremsstrahlung (IB) is the dominant laser absorption mechanism in plasma. If most of the laser energy is locally absorbed around the critical density, then isothermal expansion is a good assumption for the plasma expansion in the corona. The energy and material are injected into the corona from the laser absorption region (around the critical density). The isothermal expansion has a self-similar solution [12],

$$n = n_0 \exp(-\frac{x}{c_s t})$$

$c_s = \sqrt{\frac{ZkT_e}{M}}$ is the ion sound velocity, kT_e is electron temperature, M is the mass of ion. According to the density profiles shown in Fig. 5 we can conclude that at early time of laser pulse most the laser energy is locally deposited around the critical density, but this not is true for late time of laser pulse. This result suggests that significant laser energy is deposited over a wide region in the expanding plasma.

A typical spatial intensity distribution in the focal spot of a laser beam can be described as a Gauusian function, i.e., the highest intensity is located at center of the focal spot. So more energy is deposited at the center along the lateral direction over wide density regions along the longitudinal direction then the temperature gradient in the corona is not zero any more. The heated part will expand into both vacuum and high density regions. The faster expansion at lateral center due to higher laser intensity towards both vacuum and higher density region results in a lower density at lateral center as compared with those of outside.

We follow reference 13 to analyze the laser absorption in a plasma. The absorption length of laser light in a plasma can be described as,

$$l_{abs} = \frac{n_c}{n_e}\frac{v_g}{v_{ei}}$$

where $v_g = c\sqrt{1-\frac{n_e}{n_c}}$ is group velocity of light wave in plasma, $v_{ei} = \frac{e^4 Z n_e \ln\Lambda}{3(2\pi)^{3/2}\varepsilon_0^2 m^{1/2}(kT_e)^{3/2}}$ is electron-ion collision frequency, $\Lambda = b_{\max}/b_{\min}$ is the ratio of the impact parameters corresponding to the Debye length (b_{max} = $\lambda_D = \sqrt{\frac{\varepsilon_0 kTe}{e^2 n_e}}$) and the classic distance of the closest approach, the later can be determined by equating the energy in Coulomb field at the closest approach, $\frac{e^2 Z}{4\pi\varepsilon_0 b_{\min}}$, to the average electron thermal energy, $\frac{3}{2}mv_e^2$, $v_e = \sqrt{\frac{kTe}{m}}$ is the electron thermal velocity. The favorable temperature for efficient 13.5 nm EUV is 30 eV, and the charge state is 10. The absorption length of laser light in plasma with various densities generated by Nd:YAG (1.06 μm), and CO_2 (10.6 μm) lasers are listed in Table 1.

Table.1 Absorption length of laser light in plasma

Density	Nd:YAG (μm)	CO_2 ((μm)
$n_c/20$	100	10000
$n_c/10$	25	2500
$n_c/2$	1	100

It is seen in Table 1 that for Nd:YAG laser the laser energy can be significantly absorbed in a corona region with a length of 100 μm. This simple estimation confirms the distributed absorption in corona for short wavelength driving laser.

However the mechanism of laser deposition in a plasma substantially varies with the wavelength of the driving laser. The absorption length decreases rapidly with increasing electron density. It is seen in Table 1, for CO_2, it needs very large size low density plasma to damp laser significantly. It means that for CO_2 laser most of the laser light is always locally deposited around the critical density. With a suitable intensity, the dominant EUV emitting region is located around critical density. And because of lower density of Sn ions high CE can be expected.

The different absorption mechanism in Sn plasma with different driving laser wavelength should influence the properties of the EUV emission from the plasma. The in-band 13.5 nm EUV emission mainly comes from the unresolved transition array (UTA) from the transitions of 4d-4f of Sn^{8+} to Sn^{13+}. The bandwidth of the EUV spectrum is proportional to the charge state distribution in plasma. For Nd:YAG and short wavelength lasers, since significant laser energy is deposited at the corona, the temperature inside the corona should be not uniform over the space. The gradient of the temperature could result in broad distribution of charge state. Finally, a wide EUV spectrum is result. For CO_2 laser, the uniform temperature results in a narrower ion state distribution. So longer wavelength laser is intended to generate high purity EUV spectrum as compared with that of short wavelength. This is confirmed by the experimental results [7]. Certainly, narrower spectrum achieved by long wavelength comes from many factor in addition to the more uniform temperature, like less recombination due to low density. Since the out-band emission is not useful and worse the thermal of the EUVL system, the narrower spectrum is good for EUVL system.

3.2 Dynamics of low concentration Sn-doped foam plasma

Another key factor in the evolution of plasma is the target material. We focus on the concentration of Sn atoms. Reduction of the concentration of Sn has been shown to be an effective way to reduce Sn debris and save Sn fuel while keeping high in-band CE from laser to 13.5 nm EUV light. Sn-doped glass, Sn-doped foam, and Sn-doped water droplets have shown high CE and less debris. A Sn-doped foam spherical target with a diameter of 0.5 mm is used here. Since the diameter of the spherical target is much larger than that of the focal spot, the plasma expansion should be close to a flat target.

Plasma density of the Sn-doped foam irradiated by a Nd:YAG laser pulse was observed using the Nomarski

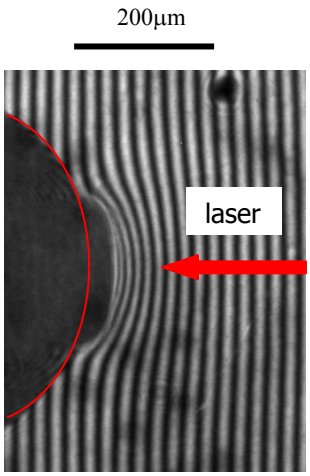

Fig.6 Interferograms of plasmas with a 0.5 % Sn-doped foam target.

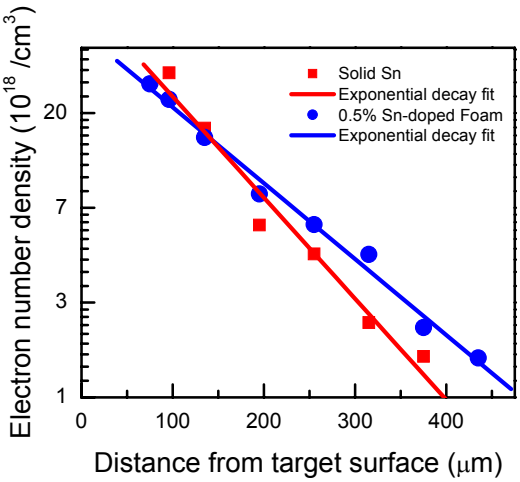

Fig.7 Density profile of plasmas with solid density Sn (red square), and 0.5 % Sn-doped foam (blue dot) targets, and the red and blue lines represent exponential decay fits.

interferometer. A typical interferograms observed at the peak of the laser pulse is shown in Fig. 6. Laser intensity is 2×10^{11} W/cm^2.

Plasma density profile along the line of laser incidence obtained from the interferograms shown in Fig. 6 with the same mathematical treatments used in pure Sn experiments is plotted in Fig.7 (blue dot). The data can be fitted by a decaying exponential function. For comparison, plasma density profile of solid density Sn observed at 0ns is also re-plotted in Fig. 7.

It is seen that the plasma density profiles of solid density Sn and 0.5 % Sn-doped foam target are almost the same except for two small differences. Since laser absorption depends on electron density, the same electron density with a low concentration Sn-doped target enables the same efficient laser energy absorption as compared with that of solid density Sn. And low concentration of Sn ions reduces the self-absorption of in-band EUV emission induced by the EUV plasma itself as compared with solid density Sn. Then even less EUV light is generated in plasma but most of it can escape the plasma. Finally, high in-band CE is result. At the same time, low concentration Sn reduces the debris from Sn and the consumption of Sn.

One difference between the plasma density profiles shown in Fig. 7 is that for the low-density foam target the highest density is located at a position closer to the initial target surface as compared with that of solid density target. This may comes from the lower density of the Sn-doped foam as compared with that of solid Sn. Another difference is the slope of the fitting line has less slope than that of solid Sn. This shows a little faster plasma expansion in the case of the low density foam target. Apparently, this comes from low average mass of C,H, and O as compared with that of solid density Sn .

4. SUMMARY

The investigation of the dynamics of laser-produced Sn plasma revealed that distributed laser absorption plays an important role in the laser plasma interaction for the short wavelength laser. Because of localized absorption and less critical density, CO_2 laser with a long wavelength is suitable to generate narrower and more efficient EUV light. Lower concentration Sn-doped foam target shows the same electron density as compared with that of solid density Sn target. The high electron density enables efficient absorption of laser light and less self-absorption of the EUV light due to less

ion density lets the EUV light efficiently escape the plasma. The combination of long wavelength laser and low concentration Sn target is worth studying in detail.

5. ACKNOWLEDGEMENTS

This research was partially supported by Cymer Inc. and by the von Liebig Center at the Jacobs School of Engineering, University of California, San Diego.

REFERENCES

1. Vivek Bakshi. EUV Sources for Lithography. SPIE Press. Bellingham, Washington USA (2005).
2. Y. Tao, S. Farshad, H. Nishimura, R. Matsui, T. Hibino, T. Okuno, S. Fujioka, K. Nagai, T. Norimatsu, K. Nishihara, N. Miyanaga, and Y. Izawa, A.Sunahara and T.Kawamura. Appl.Phys.Lett. 85, 1919(2004).
3. Y. Shimada, H. Nishimura, M. Nakai, K. Hashimoto, M. Yamaura, Y. Tao, K. Shigemori, T. Okuno, K. Nishihara , T. Kawamura , A. Sunahara , S. Fujioka, S. Uchida, N. Miyanaga, Y. Izawa and C. Yamanaka. Appl.Phys.Lett. 86, 051501(2005).
4. Michiteru Yamaura et al., Appl. Phys. Lett. 86, 181107 (2005)
5. Yoshifumi Ueno et al. Appl. Phys. Lett. 90, 191503 (2007)
6. Aghapi G. Mordovanakis, Kai-Chung Hou, Yu-Chung Chang, Ming-Yuan Cheng, John Nees, Bixue Hou, Anatoly Maksimchuk, Gerard Mourou, Almantas Galvanauskas, and Bruno Lafontaine. Opt. Lett. 31, 2517 (2006)
7. Igor V. Fomenkov et al. Proc. SPIE 6517, 65173J (2007)
8. S. S. Harilal, M. S. Tillack, Y. Tao, B. O'Shay, R. Paguio and A. Nikroo. Optics Letters, 31, 1549 (2006)
9. Y. Tao, M.S.Tillack, S.S.Harilal, K.L.Sequoia, and F.Najmabadi. J. Appl. Phys., 101, 023305 (2007)
10. R.R. Paguio, C.A. Frederick, J.F. Hund, D.G. Czechowicz, A. Nikroo, M. Takagi, O. Acenas, and M. Thi. Fusion Engineering 2005, Twenty-First IEEE/NPS Symposium on Fusion Engineering, Sept. 2005, Knoxville, TN
11. http:/optics.tu-graz.ac.at/
12. William L. Kruer. The Physics of Laser Plasma Interaction. Addison-Wesley, California, USA(1988).
13. David Attwood. Soft x-rays and Extreme Ultraviolet Radiation. Cambridge University Press, Cambridge UK (1999).